



Improved site-dependent statistical relationships of V_s and resonant frequency versus bedrock depth in Japan

Mostafa Thabet

Received: 3 May 2021 / Accepted: 5 August 2021 / Published online: 26 September 2021
© The Author(s), under exclusive licence to Springer Nature B.V. 2021

Abstract Combining both processing techniques of horizontal-to-vertical spectral ratio (HVSR) and surface-to-borehole spectral ratio (SBR), using the KiK-net and K-NET database in Japan, could be used in the present study to establish relationships of V_s and resonant frequency (f) versus depth to bedrock half-space (h) based on the site-dependent variability. Remarkable correlations of the average V_s of layers overlying the bedrock half-space ($\overline{V_s}$) versus h are inversely resembling those of the f versus h . The maximum $\overline{V_s}$ values are 1262 m/s, 933 m/s, 842 m/s, and 568 m/s through site class of B, C, D, and E, respectively. These values of $\overline{V_s}$ are decreasing gradually resembling the V_{s30} through site class of B, C, D, and E according to (NEHRP, Report FEMA 368, NEHRP, Washington, 2000). The f versus h regressions at KiK-net sites yield gradual decrease

in the correlation coefficients (i.e., a and b) through site class of B, C, D, and E, particularly the resulted a and b from SBR technique. K-NET sites yield significant lower correlation coefficients, which could be attributed to the K-NET shallow depths (h) and their corresponding limited ranges of (f). Although such relationships are site-specific and highly dependent on each region's geologic conditions, fair comparisons based on site information and site-dependent variability between previous relationships of f versus h in the literature and the present study relationships are showing remarkable similarities. This indicates significant importance of introducing the seismic site classification as a crucial controlling factor in establishing the previous and the present V_s and f versus h nonlinear regression relationships.

Supplementary Information The online version contains supplementary material available at <https://doi.org/10.1007/s10950-021-10038-9>.

M. Thabet (✉)
Geology Department, Faculty of Science, Assiut University, Assiut 71516, Egypt
e-mail: mostafa.thabet@aun.edu.eg
URL: <https://life.aun.edu.eg/science/mostafa-thabet-mohamed-thabet>; <https://scholar.google.com/citations?user=wPsYhrMAAAJ&hl=en>; http://www.researchgate.net/profile/Mostafa_Thabet2

M. Thabet
Disaster Prevention Research Institute (DPRI), Kyoto University, Kyoto, Japan

Keywords Horizontal-to-vertical spectral ratio · Transfer function · Resonant frequency · Bedrock depth · S -wave velocity · Seismic site classification · KiK-net and K-NET (Japan)

1 Introduction

The statistical nonlinear regression relationships of the fundamental resonant frequency (f) and S -wave velocity (V_s) versus bedrock depth (h) are usually used to estimate the depth to the bedrock half-space. The general form of the relationship of f versus h could be defined as

$$h = af^{-b} \quad (1)$$

where a and b are correlation coefficients.

Based on microtremor observation, the characteristics of ground motions could be estimated using the pioneering horizontal-to-vertical spectral ratio (HVSR) technique by Nakamura (1989). Henceforward, Lermo and Chavez-Garcia (1993) and Wen et al. (2006) estimated the fundamental resonant frequency using HVSR of weak and strong earthquakes. Recently, Sánchez-Sesma et al. (2011) back-calculated the 1D velocity structure applying the diffuse field theory on HVSRs of microtremors, whereas Kawase et al. (2011) and Nagashima et al. (2014) used the HVSRs of earthquake recordings. Long-period microtremor measurements by Yamanaka et al. (1994) concluded that the resulted Rayleigh waves ellipticities are resembling those resulted from earthquakes. Their study was conducted in the north-western part of the Kanto Plain, Japan. Moreover, the HVSRs of ambient vibrations fit well with the resulted fundamental frequencies of standard spectral ratios of earthquakes (Bard and SESAME team 2004).

In the literature, previous existing relationships of f versus h were determined based on HVSRs of microtremor investigations (e.g., Ibs-von Seht and Wohlenberg 1999, Delgado et al. 2000a and 2000b, Parolai et al. 2002, Scherbaum et al. 2003, Hinzen et al. 2004, García-Jerez et al. 2006, D'Amico et al. 2008, Harutoonian et al. 2013, Tün et al. 2016, and Moon et al. 2019). Using earthquakes of KiK-net to determine regression relationships of f versus h is examined by Thabet (2019). These statistical nonlinear regression relationships are highly site dependent.

Early introduction of the empirical transfer function (ETF) in the valuable study conducted by Borchardt (1970) is considered as the base of other later studies. Calculating the ETF is usually done using a standard spectral ratio (SSR), and requires a pair of instruments, one located at a surface soil site under investigation (generally on alluvium) and the other at a nearby surface reference rock site. The ETF represents resonant frequencies of the soil column. These resonant frequencies are only descriptive of that portion of the soil column between the two sensors and are not necessarily representative of the site's global behavior experienced by an earthquake event. Pioneering study of Kagami et al. (1982)

examined the usefulness of long-period microtremor observations in Niigata plain, Japan, and in Los Angeles, California. Their results showed that Fourier amplitude of microtremors systematically increase from shallow to deep sites resembling observation from strong-motion earthquake records during the Niigata earthquake of 1964 and the San Fernando earthquake of 1971. Satoh et al. (1995) conducted their study to evaluate the local site effects due to surface layers overlying the engineering bedrock and to remove them by using one-dimensional (1D) soil models. They could estimate the engineering bedrock waves, which are supposed to be observed on the outcrop of the engineering bedrock, from borehole records. They concluded that the resonant frequency determined from SBR at a borehole site should not be treated as the resonant frequency of the site. Microtremor measurements were carried in the western lower Rhine embayment (Germany) by Ibs-von Seht and Wohlenberg (1999) to estimate the resonance frequency using the classical spectral ratios and taking advantage of hard rock basement sites used as reference stations. Horike et al. (2001) compared the relative amplification factors inferred from HVSRs of microtremor and earthquake motions, and they found reasonable agreement between the resulted spectral ratios. Satoh et al. (2001a) conducted 48 single stations and 12 arrays of microtremor measurements in Taichung Basin, Taiwan. They estimated the S -wave velocity structure using the Rayleigh wave inversion technique by matching the calculated Rayleigh wave HVSR to observed HVSR.

In the present study, the surface-to-borehole spectral ratios (SBRs) are calculated using database of the Kiban Kyoshin network (KiK-net) in Japan. Seismic downhole array sites of KiK-net are invaluable tools in the present attempts to understand and accurately estimate the fundamental resonant frequency (f). Ground motions recorded at various depths within these seismic vertical arrays are used to calculate the surface-to-borehole spectral ratios (SBRs), and consequently estimate the peak frequencies as the seismic waves travel from bedrock half-space to the ground surface. When using recorded ground motions from vertical seismic arrays (i.e., surface and borehole records), it is nearly inevitable to separate between the down-going and up-going seismic wave effects. Tao and Rathje (2020) showed clearly that both effects are not negligible. They examined the

down-going wave effect and the appearance of pseudo-resonances in downhole array data for sites with a shallow velocity contrast or with little to no velocity contrast. In contrast to this study, Rong et al. (2016) compared HVSRs of the S -wave with one dimensional equivalent-linear numerical simulations on 21 sites in western China and suggested that the HVSR from observed earthquake ground motion resembles the SBR of nonlinear site response. Therefore, it is recommended to carefully select sites, which have similar SBR and HVSR, to avoid the down-going and up-going seismic wave effects.

Thabet (2019) determined site-dependent regression relationships of h versus f using HVSRs of earthquakes at KiK-net sites, Japan. Although the resulted HVSR peak frequencies are clear, unique, and sharp, there is a dominated strong scattering in the relationships of h versus f up to bedrock depths of 100 m. Some KiK-net sites are excluded from the study conducted by Thabet (2019) due to their strong non-stationary behavior, which lead to high scattering and perturbations in their resulted HVSRs. According to Thabet (2019), there are 192 having their bedrock depths < 20 m, which corresponds to 59.3% of the accepted 324 KiK-net sites. This means that bedrock depths < 20 m are significantly responsible for the high scattering, which is dominated in the relationships of h versus f up to bedrock depths of 100 m. Moreover, these 192 sites constitute approximately 27.5% of the whole 698 KiK-net sites. So that, it is expected to obtain ≈ 287 accepted K-NET sites out of the whole 1045 K-NET sites in the present HVSR analyses. For that reason, both KiK-net and K-NET sites in Japan are used in the present study. The fundamental resonant frequency is determined using HVSR and SBR analyses (i.e., f_{HVSR} and f_{SBR} , respectively) at KiK-net sites, whereas only f_{HVSR} is determined at K-NET sites. In total, all the available earthquake records from 1997 to 2019 at 698 KiK-net and 1045 K-NET seismic sites are used. Borchardt (1994) stated that time average S -wave velocity of the upper 30 m (V_{s30}) provides accurate site characterization and permits seismic site classification unambiguously. S -wave velocity of the upper 30 m (V_{s30}) is the main factor for the seismic site classification in terms of seismic response by many organizations, particularly the National Earthquake Hazard Reduction Program (NEHRP). In this study, site-dependent

relationships of f_{HVSR} , f_{SBR} , and S -wave velocity (V_S) versus h in Japan are provided for more improvement to reveal the influence of different physical and geological parameters on these statistical site-specific nonlinear regression relationships. Additionally, the applicability and discrepancy between HVSR and SBR are revealed and discussed.

2 Data set

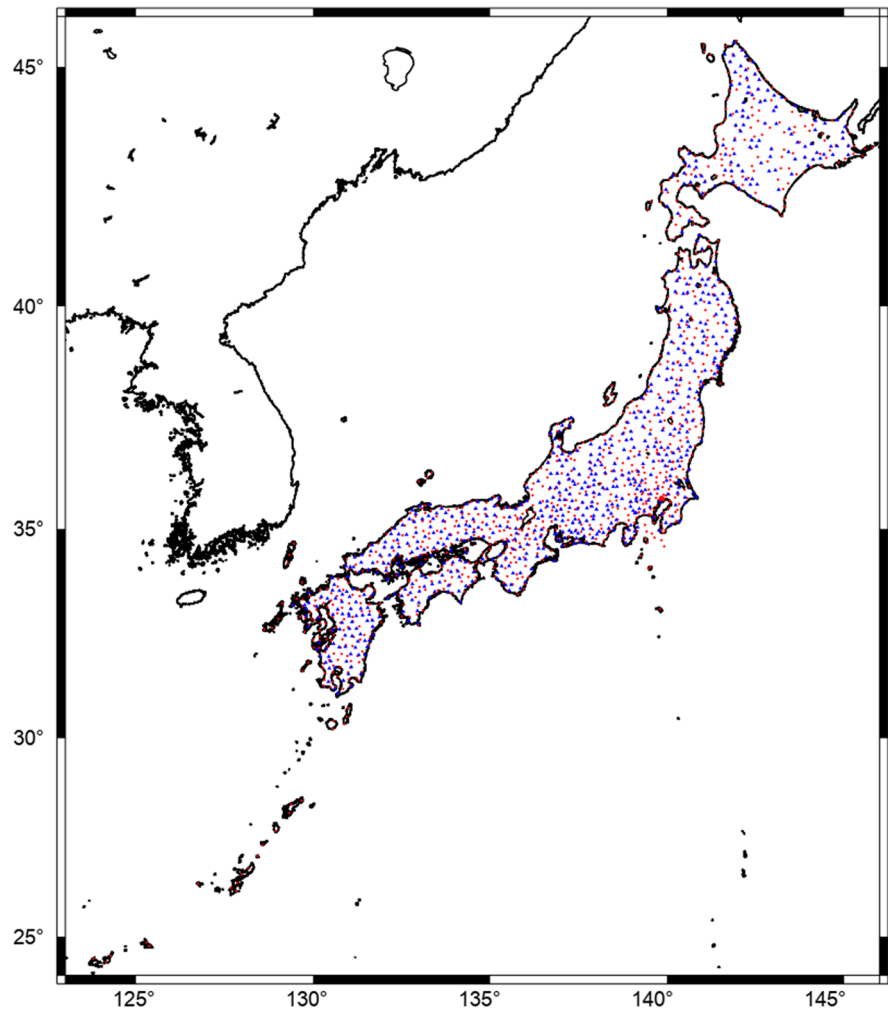
The data from the KiK-net and K-NET in (last accessed, January 2020) Japan are used to establish the proposed statistical nonlinear regression relationships based on the seismic site classification. The KiK-net consists of 698 seismic vertical array sites equipped with a pair of surface and borehole accelerometers, and the K-NET consists of 1045 sites equipped with seismic surface accelerometers (refer to Fig. 1).

KiK-net site data have high variety of stratigraphic and lithologic columns and V_P and V_S structures up to depths between 100 and 3500 m. Around 88% of KiK-net sites have borehole depths up to 250 m, whereas 12% have their borehole depths (250–500 m) and higher than 500 m, equally. As a result, it will be possible to define the bedrock half-space.

The K-NET consists of 1045 strong-motion observation sites with a spacing of 25 km. This spacing of the K-NET is essential to record strong motions in the epicentral region of a crustal earthquake with more than magnitude of 7 anywhere in Japan. Beneath each K-NET site, the observed detailed N -value (i.e., blow count of standard penetration test), V_P and V_S structures, bulk densities (ρ), and lithologic column are provided down to a depth of 20 m. The vertical resolution of these observed data is 1 m. These observed data are a valuable opportunity to test and experience the present strong scattering that is dominated in the regression relationships of h versus f at bedrock depths of < 30 m. Those KiK-net and K-NET sites show very wide lithological variation.

All KiK-net and K-NET sites are classified according to the definition of National Earthquake Hazards Reduction Program (NEHRP Provision, 2000) site classes. According to Boore (2004), there are common three extrapolation methods to estimate the V_{s30} , and consequently it will be possible to

Fig. 1 Location map of KiK-net and K-NET seismic stations. Blue triangles are the 698 KiK-net seismic sites. Red circles are the 1045 K-NET seismic sites



classify K-NET sites having shallow velocity models of depths < 30 m according to the NEHRP seismic site class. These extrapolation methods are (1) assuming constant velocity, (2) using the correlation between V_{S30} and $\overline{V}_S(d)$, and (3) based on velocity statistics to determine site class. In the present paper, the simplest method is adapted, which is assuming that the lowermost velocity of the model extends to 30 m (see Eq. 2).

$$V_{S30} = 30 / (t(d) + \frac{30 - d}{V_{eff}}) \quad (2)$$

where V_{eff} is the assumed effective velocity (i.e., velocity at the bottom of the velocity model) from the bottom depth of K-NET site (d) to 30 m. $t(d)$ is the travel time to a depth d .

The most of KiK-net and K-NET sites have a class of C or D. Minority of the sites has a class of B or E, whereas sites have a class of A are not involved. In the present study, the KiK-net and K-NET enormous earthquake database collected covers the period between 1997 and 2019. Waveforms are recorded with a sampling frequency of 100 Hz for most of the used events and 200 Hz for some events. All the available events with PGAs (i.e., Peak Ground Accelerations) of ≤ 10 cm/s^2 are used in the present analyses in accordance with Régnier et al. (2013) in order to characterize the linear behavior at each site. This implied that linear behavior is prevailing avoiding later modification due to nonlinear response (Thabet et al. 2008 and Thabet 2021). This enormous earthquake database for each KiK-net and K-NET site is prepared using multiple earthquakes approach (Thabet 2019),

and is simply assuming several consequent earthquake records as a continuous time series to lengthen the total time window of each record. Between each two adjacent earthquake records, the effect due to conjunction points is negligible because the frequencies of interest are low (i.e., ≤ 50 Hz). Figure 2 shows an example of 737-earthquake surface records at IBRH15 site. Adopting multiple earthquake approach enable us to exclude sites having recorded earthquakes with strong non-stationary and may undergo high scattering and perturbations, which may significantly affect the physical meaning of the HVSR and SBR peak frequencies. As a result, the included or accepted sites in the present study have the lowest level of scattering (i.e., acceptable low standard deviation values) indicating that propagation path effects, which are represented in shallow or deep earthquakes and far-field or near-field earthquakes, could not control the resulted HVSR or SBR curves.

3 Methods of analyses

The HVSR technique (Nogoshi and Igarashi 1970 and 1971; Nakamura 1989 and 2000) has been extensively studied with earthquake recordings to quantify the site effect produced by the sedimentary covering in specific frequency bands (Field and Jacob 1993; Lachet and Bard 1994; Lermo and Chavez-Garcia 1994; Bindi et al. 2000; Fäh et al. 2001). The HVSR is defined as the ratio of the quadratic mean of horizontal Fourier amplitude of ground motion (i.e., EW and NS components) and the vertical Fourier amplitude of ground motion at the free surface. The calculation is illustrated in

$$HVSR = \frac{\sqrt{(EW^2 + NS^2)/2}}{V} \tag{3}$$

where EW , NS , and V are the acceleration Fourier amplitude spectra of the east–west, north–south, and vertical components of the ground motion, respectively.

GEOPSY software suite (<http://www.geopsy.org>) is used for HVSR processing the prepared conjugated three-component events at the surface of each KiK-net and K-NET site. These lengthy time-window conjugated records provide fulfillment of the widely accepted framework guidelines of the European research project SESAME (Bard and SESAME team 2004). These guidelines have been consulted and followed concerning HVSR processing. Therefore, the reliability and quality of these HVSR calculations are assessed depending on three basic requirements. They are the following: (a) the expected fundamental resonant frequency of interest must be more than 10 significant cycles in each time window, (b) the total number of the significant cycles must be more than 200 and it is recommended to be raised around two times at low fundamental resonant frequencies, and (c) the acceptable low standard deviation values that are calculated for the amplitudes of the time windows, which is recommended to be less than 2 for peak frequencies higher than 0.5 Hz or 3 for peak frequencies lower than 0.5 Hz. The identification of the clear peak frequency (f_0) is met when the HVSR curve exhibits two quantitative criteria for a clear HVSR peak frequency as proposed by Bard and SESAME team (2004). Those criteria are the amplitude and stability conditions. Table 1 is summarizing the threshold values of amplitude and frequency.

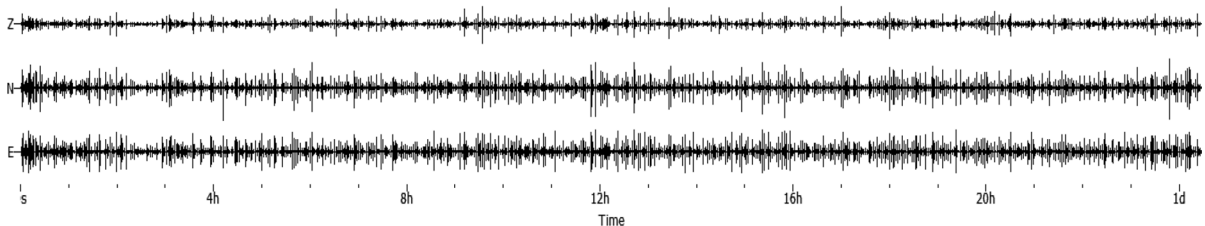


Fig. 2 Example of more than 1-day time window of the conjugated three components (i.e., Z, N, and E are UD, NS, and EW components, respectively) of 737 events recorded at IBRH15 site prepared for processing in GEOPSY software suite. (Note:

the shown 737 earthquake events are all the recorded events at IBRH15 site from 1997 to 2019 with amplitudes less than 10 cm/s²)

Table 1 Threshold parameters for the identification of a clear peak frequency according to guidelines by Bard and SESAME team (2004)

(σ_f)	$\pm 5\%$				
Amplitude (A_0) of peak frequency	> 2				
Peak frequency range (Hz)	< 0.2	$0.2\text{--}0.5$	$0.5\text{--}1.0$	$1.0\text{--}2.0$	> 2.0
$\varepsilon(f_0)$ (Hz)	$0.25 f_0$	$0.20 f_0$	$0.15 f_0$	$0.10 f_0$	$0.05 f_0$
$\theta(f_0)$ for $\sigma_A(f_0)$	3.0	2.5	2.0	1.78	1.58

Amplitude conditions require that the HVSR amplitude of the peak frequency must be higher than 2 (i.e., $A_0 > 2$). The stability conditions require the following: (1) the peak frequency should appear at the same frequency on the HVSR curves corresponding to mean+ and –one standard deviation (i.e., σ_f is within a percentage $\pm 5\%$) of the peak frequencies estimated from individual time windows of the orthogonal components at one KiK-net or K-NET site, (2) σ_f (i.e., standard deviation of f_0 estimated from individual time windows) must be lower than a frequency-dependent threshold $\varepsilon(f)$, and (3) $\sigma_A(f_0)$ (i.e., standard deviation of the HVSR amplitudes of the peak frequencies estimated from individual time windows) must be lower than a frequency-dependent threshold $\theta(f)$.

A seismogram can be visualized as the convolution of the source effect, propagation path effect, site effect, and instrument response as

$$A_{ij}(t) = S_i(t) * P_{ij}(t) * G_j(t) * I_j(t) \tag{4}$$

where $S_i(t)$ is the source effect, $P_{ij}(t)$ is the propagation path effect, $G_j(t)$ is the site effect, $I_j(t)$ is the instrument response, of the i th event, and for the j th station at free surface. “*” denotes the convolution operator.

Denoting Fourier transform, Eq. 4 can be written as in Eq. 5. The spectral ratio is obtained by dividing the Fourier spectrum of the acceleration at the j th station at free surface by the spectrum at the k th station at borehole as in Eq. 6.

$$A_{ij}(f) = S_i(f)P_{ij}(f)G_j(f)I_j(f) \tag{5}$$

$$\frac{A_{ij}(f)}{A_{ik}(f)} = \frac{S_i(f)P_{ij}(f)G_j(f)I_j(f)}{S_i(f)P_{ik}(f)G_k(f)I_k(f)} = \frac{G_j(f)}{G_k(f)} \tag{6}$$

If the distance between stations j and k is much less than their hypocentral distances from the

source, the source and path effects would be eliminated. The instrument response can be removed assuming similar instrument units at surface and in borehole. The exact site response can thus be obtained from Eq. 6.

In this study, SBR is defined as spectral ratios between the acceleration horizontal Fourier amplitude motions recorded on the free surface and in the borehole at each KiK-net site. Equations 7 and 8 show the SBR of both horizontal components (i.e., EW and NS, respectively).

$$SBR_{ew} = H_{s,ew}/H_{b,ew} \tag{7}$$

$$SBR_{ns} = H_{s,ns}/H_{b,ns} \tag{8}$$

where “s” and “b” terms are referred to motions recorded on the free surface and in the borehole, respectively.

The Fourier amplitude spectra for surface and borehole horizontal components at each KiK-net site are calculated using GEOPSY software suite (<http://www.geopsy.org>). Fulfilling Bard and SESAME team (2004) guidelines, the reliability and quality of the SBR calculations are also assessed depending on the previously explained three basic requirements. As a result, f_{SBR} could be estimated for both horizontal components (EW and NS) and defined as f_{SBR-EW} and f_{SBR-NS} , respectively. Calculating the f_{SBR-EW} and f_{SBR-NS} is carried out for two reasons. The first reason is to estimate the effects of lateral or horizontal variation in the lithology. The second reason is to estimate the directional or structural control dependency on site resonance.

Previous work by Ibs-von Seht and Wohlenberg (1999) defined the bedrock depths based on the interface between the soft sedimentary covers of different thicknesses of Tertiary and Quaternary ages ($V_S < 1000$ m/s), and Paleozoic hard rock basement ($V_S \geq 2500$ m/s). Delgado et al. 2000a, 2000b(a)

defined the bedrock depths based on the interface between the Upper Miocene sedimentary fill (i.e., conglomerates, sandstones, and marls) of Bajo Segura basin ($V_S \geq 85$ m/s), and the basement of the basin which is composed of limestones and marls of Triassic to Cretaceous age ($V_S \geq 200$ m/s). Özalaybey et al. (2011) depended on geological evaluation and gravity data to estimate the bedrock depths in Izmit basin. García-Jerez et al. (2006) estimated the sedimentary cover thicknesses (i.e., depth to bedrock half-space) in Zafarraya basin by means of close geoelectrical surveys. Thabet (2019) estimated h at a site based on the highest seismic impedance ratio between each adjacent underlying and overlying layers. In this study, h is estimated at each KiK-net and K-NET site according to the highest seismic reflection coefficient of V_P and V_S (i.e., IC_P and IC_S) between each adjacent two layers, which are calculated based on the concept of seismic reflection coefficient (see Eqs. 9 and 10). So that, it will be possible to identify the presence of high velocity layer, which has negative IC_P and/or IC_S . Consequently, bedrock presence could be clearly judged and differentiated from the presence of high velocity layer.

$$IC_P = \frac{(\sigma V_P)_{i+1} - (\sigma V_P)_i}{(\sigma V_P)_{i+1} + (\sigma V_P)_i} \tag{9}$$

$$IC_S = \frac{(\sigma V_S)_{i+1} - (\sigma V_S)_i}{(\sigma V_S)_{i+1} + (\sigma V_S)_i} \tag{10}$$

where σ is the density of each layer i (note: 1 is the surficial layer and i th for underlying layers).

The appropriate h is assigned to its f_{HVSR} and f_{SBR} , whereas the unreasonable h is excluded from any further analyses due to difficulties or suspicion in assigning the accurate and proper bedrock half-space. However, exclusion of KiK-net and K-NET sites from further analyses is executed depending on designed filtering process as illustrated in Fig. 3 and Fig. 4, respectively. The rejected or excluded sites from further analyses are due to many reasons. They are organized on a base of step-by-step process as follows: (1) the unavailability of velocity structures, geotechnical, or seismological database at some KiK-net and K-NET sites, (2) K-NET sites exhibiting peak resonance frequencies < 2.5 Hz, (3) the clarity criteria according to SESAME guidelines (Bard and SESAME team 2004) is not satisfied, (4) presence

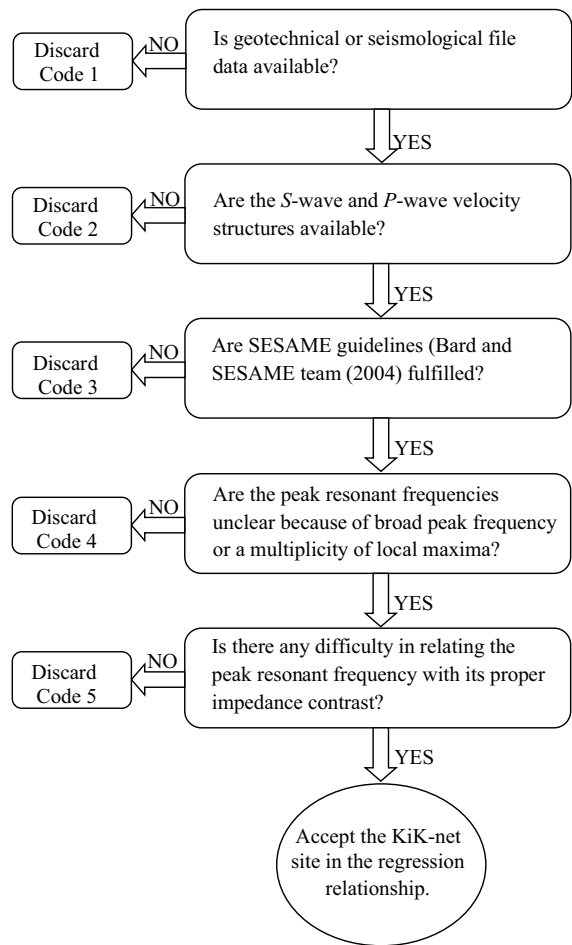


Fig. 3 Flowchart showing the designed filtering process to discard or accept KiK-net site in the present regression relationship

of unclear peak frequency such as broad peak frequency or a multiplicity of local maxima, and (5) difficulties in relating the peak resonance frequency with its proper seismic reflection coefficient bedrock half-space. The present PS logging seismic velocity structures of KiK-net and K-NET are considered as reliable and applicable (Thabet 2019).

4 Results and discussion

Out of 698 KiK-net sites processed with HVSR and SBR methods and 1045 K-NET sites processed with HVSR method, 366 and 483 KiK-net sites processed with HVSR and SBR, respectively, and 339 K-NET

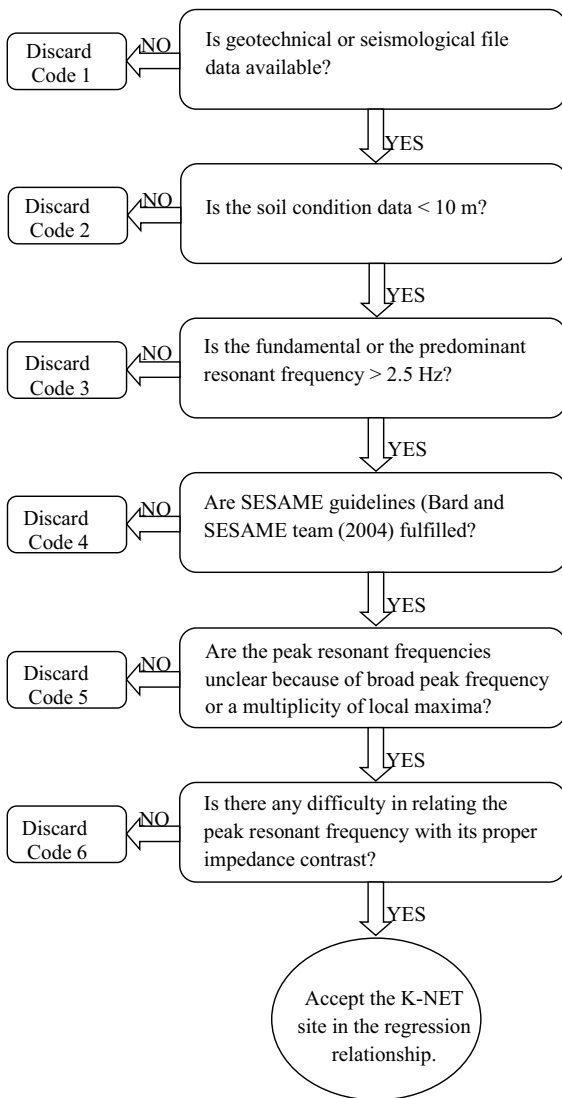


Fig. 4 Flowchart showing the designed filtering process to discard or accept K-NET site in the present regression relationship

sites processed with HVSR method could be accepted and included in the further analyses. Table 2 shows the ranges of h and f of the accepted sites in the present study. Interesting investigation is carried out by Zhu et al. (2020) at 90 KiK-net sites, which have no large velocity contrast. They perform novel empirical correction to preserve the earthquake HVSR with that of one-dimensional S -wave amplification spectrum. As a result, the observed ETF, which could be taken as SBR, could be reproduced. Figure 5 is showing two comparisons between $f_{HVSR-KiK}$ versus

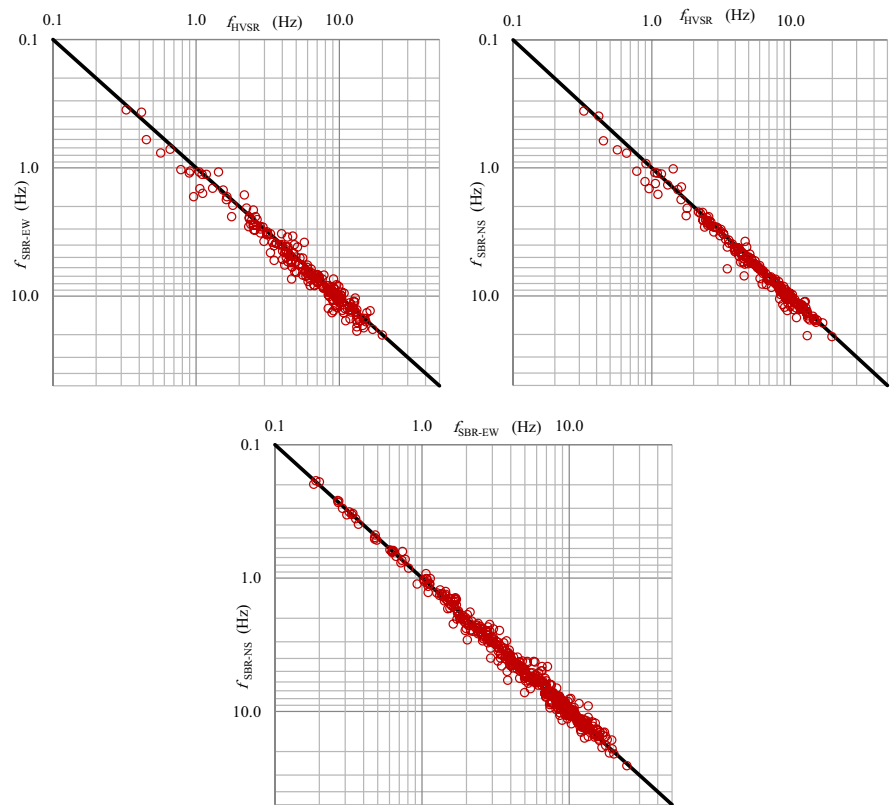
Table 2 Resulted ranges of h and f in the present study

	Min. f (Hz)	Max. f (Hz)	Min. h (m)	Max. h (m)
HVSR KiK-net	0.16	25.28	1	1000
SBR KiK-net	0.18	25.00	1	1350
HVSR K-NET	2.54	26.35	1	18

f_{SBR-EW} and f_{SBR-NS} . Both comparisons are based on the same KiK-net sites having accepted $f_{HVSR-KiK}$, f_{SBR-EW} , and f_{SBR-NS} . f_{SBR-EW} and f_{SBR-NS} tend to be equal to or slightly higher than their corresponding $f_{HVSR-KiK}$. This indicates that f_{SBR-EW} and f_{SBR-NS} are comparable to their corresponding $f_{HVSR-KiK}$. Moreover, the variability between SBR_{ew} and SBR_{ns} is tested through comparison between f_{SBR-EW} and f_{SBR-NS} as shown in Fig. 5. This indicates that the lateral variation between EW and NS components considering the resonance peak frequencies are insignificant, particularly for sites having peak frequencies < 1 Hz. For that reason, the arithmetic average between SBR_{ew} and SBR_{ns} is calculated and the f_{SBR} is used henceforward. Figure 6 shows that the class of C and D are the dominant site classes as depicted from the accepted KiK-net and K-NET sites.

The engineering bedrock has S -wave velocity of 400 to 700 m/s according to seismic microzonation study by Nath (2007), while Miller et al. (1999) defined the bedrock by considering S -wave velocity of ≥ 244 m/s using MASW survey. Delgado et al. (2000b) defined the geotechnical bedrock by considering S -wave velocity > 250 m/s of the Triassic carbonate rocks and Triassic to Cretaceous limestones. However, the engineering bedrock has S -wave velocity of ≥ 350 m/s, whereas the seismological or seismic bedrock corresponds to S -wave velocity of ≥ 3000 m/s (Satoh et al. 2001b, Kawase et al. 2011 and Kawase et al. 2018). In the present paper, 302 and 37 out of the 339 K-NET sites processed with HVSR method have S -wave velocity of bedrock > 350 –2000 m/s and < 350 m/s, respectively. 348 and 18 out of the 366 KiK-net sites processed with HVSR method have S -wave velocity of bedrock > 350 –3000 m/s and < 350 m/s, respectively, whereas 453 and 30 out of the 483 KiK-net sites processed with transfer function method

Fig. 5 Comparison between fundamental resonant frequencies resulted from SBR, of both horizontal EW and NS components, and HVSR at KiK-net sites



have *S*-wave velocity of bedrock > 350–3000 m/s and < 350 m/s, respectively. As a result, those minor sites with *S*-wave velocity of bedrock < 350 m/s have intermediate layer within the sediments (i.e., highest seismic reflection coefficient interface)

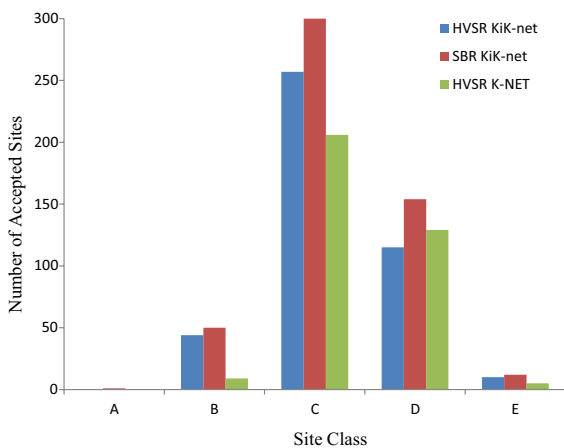


Fig. 6 Statistics of the accepted sites resulted from HVSR and SBR classified according to NEHRP Provision (2000)

and responsible for producing peak resonance frequency.

Figure 7 shows three examples of KiK-net sites that are producing clear sharp and unique single HVSR and SBR fundamental resonant frequencies of > 3 Hz, 1–3 Hz, and < 1 Hz that are processed at SZOH34, YMTH15, and ISKH06 sites, respectively. In the supplementary material, Figures S1 through S10 are showing various examples of KiK-net sites processed with HVSR and SBR and K-NET sites processed with HVSR. The examples exhibit clear, sharp, and unique single HVSR or SBR peak frequencies. Figures S11, S12, and S13 are showing various examples of discarded KiK-net sites processed with HVSR and SBR and K-NET sites processed with HVSR. Tables S1, S2, and S3 are showing the whole discarded KiK-net and K-NET sites with their discard codes. There are 23 KiK-net sites and 34 K-NET sites with no available velocity structure or any geotechnical database. Four K-NET sites have their soil condition data to a depth of only 5 m. Due to the depth limitation in K-NET database to ≤ 20 m, so that, 388 K-NET sites are discarded because they have peak resonance

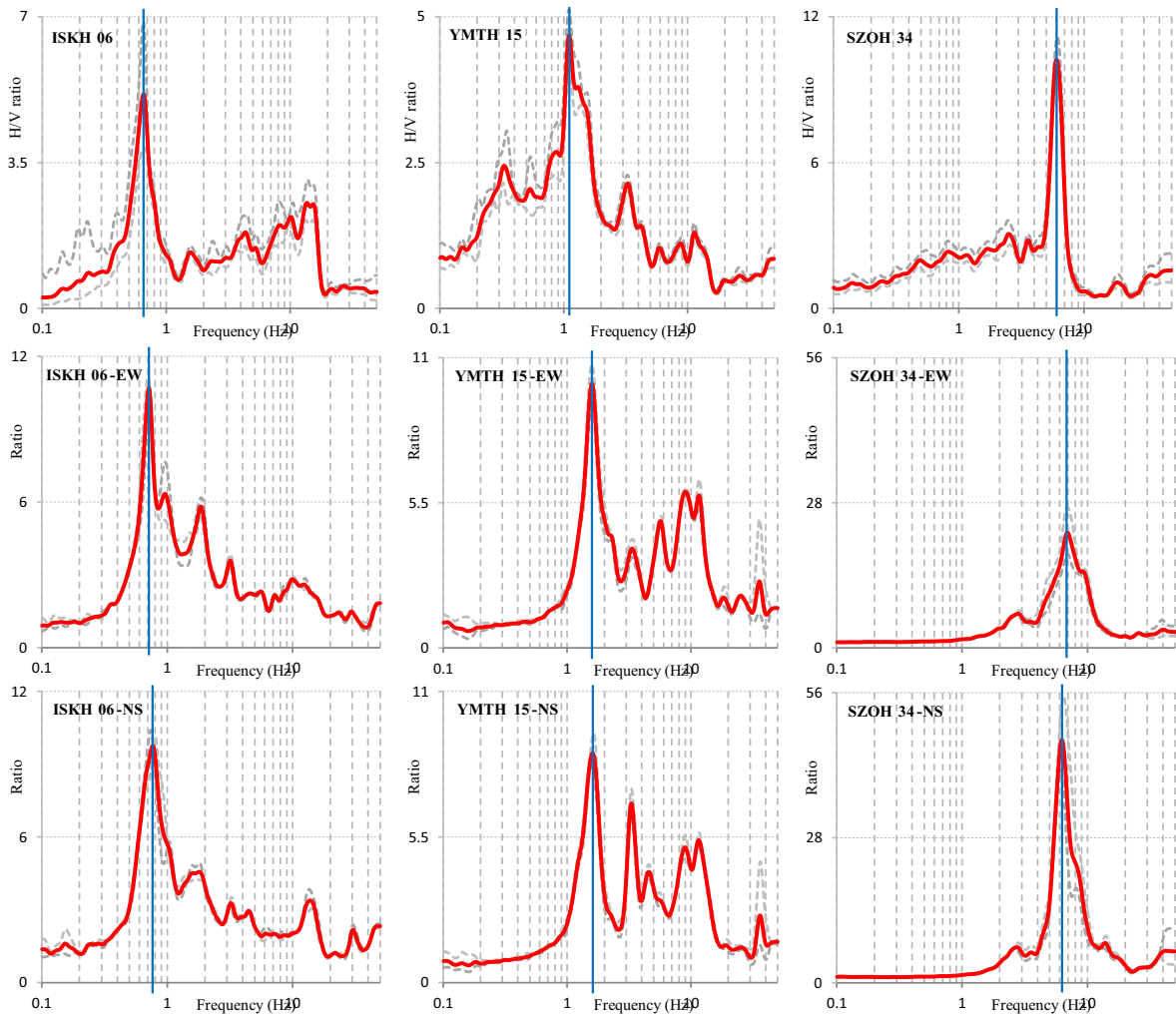


Fig. 7 Examples of peak frequencies at ISKH06, YMTH15, and SZOH34 KiK-net sites resulted from HVSR (upper curves) and SBR of both horizontal components (middle and lower

curves). (Note: red curves are the average HVSR or SBR curves, whereas the pale gray curves are the minimum and maximum)

frequency < 2.5 Hz which is corresponding to > 20 m depth. There are 291, 106, and 197 KiK-net sites processed with HVSR and SBR and K-NET sites processed with HVSR, respectively, not satisfying the clarity criteria according to SESAME guidelines (Bard and SESAME team 2004). Discarded 7, 62, and 21 KiK-net sites processed with HVSR and SBR and K-NET sites processed with HVSR, respectively, have unclear peak frequency such as broad peak frequency or a multiplicity of local maxima. Due to difficulties in relating the peak resonance frequency with its proper seismic reflection coefficient bedrock half-space, 11, 24, and 62 KiK-net sites processed

with HVSR and SBR and K-NET sites processed with HVSR, respectively, are discarded. It is important to know that Thabet (2019) used 324 KiK-net sites processed with HVSR method, whereas the present study could success to increase the accepted or included sites up to 366 KiK-net sites processed with HVSR method. This improvement is due to adopting multiple earthquake approach, which enable us to include all the available ground motion records with PGAs ≤ 10 cm/s². Consequently, the effect of strong non-stationary nature of waveforms, which may significantly affect the physical meaning of the HVSR and SBR, could be minimized or eliminated in the

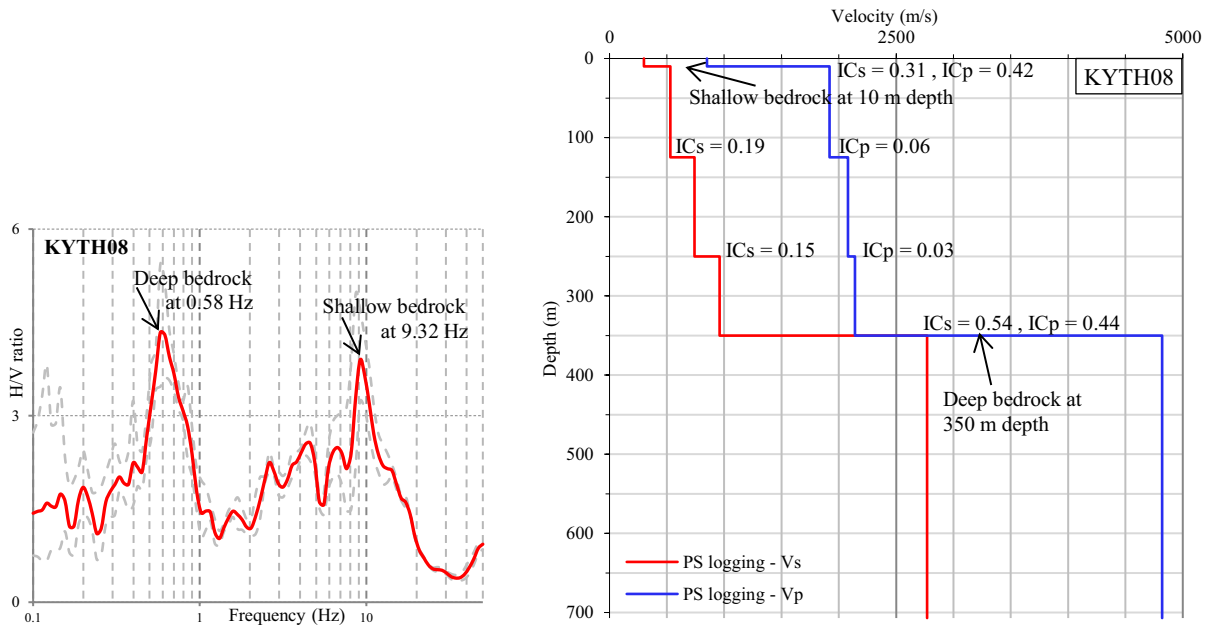
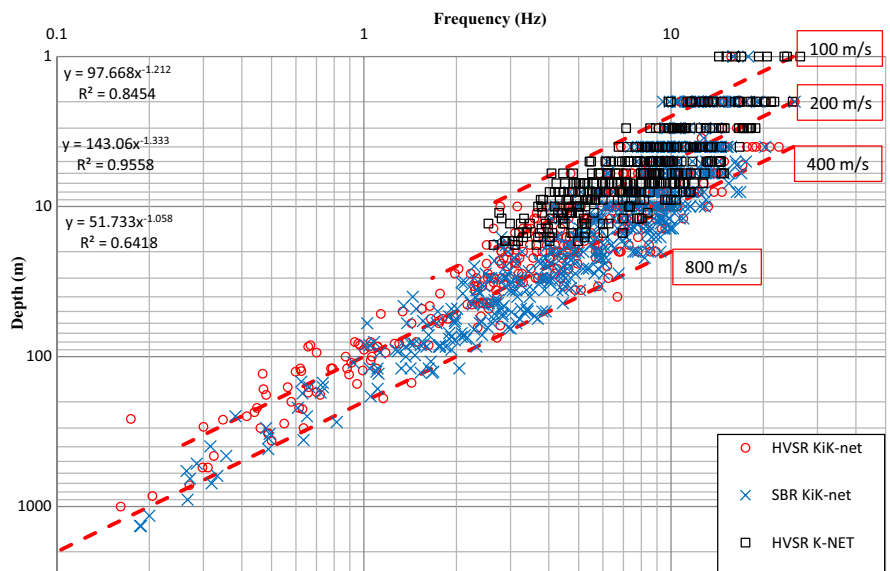


Fig. 8 Example of bedrock depth assignment at KYTH08 site

resulted peak frequencies. The other improvement in the present study is the accepted or included 483 KiK-net sites processed with SBR. As depicted from Eq. 6, SBR proves its efficiency in assessing the site response based on surface-to-borehole KiK-net sites. This indicates the applicability and productivity of SBR method in establishing regression relationships of h versus f .

Figure 8 shows an example of assigning the HVSR fundamental and secondary resonant frequencies to their deep and shallow bedrock half-spaces, respectively, at KYTH08 KiK-net site. In this example, the first highest IC_p and IC_s are directly indicating the deep bedrock half-space at 350 m depth, whereas the second highest IC_p and IC_s are directly indicating the shallow bedrock half-space at 10 m depth. As shown

Fig. 9 Fundamental resonant frequency versus bedrock depth obtained from HVSR and SBR of KiK-net sites and from HVSR of K-NET sites. (Nonlinear regression equations from top to bottom are corresponding to HVSR and SBR of KiK-net, and HVSR of K-NET, respectively)



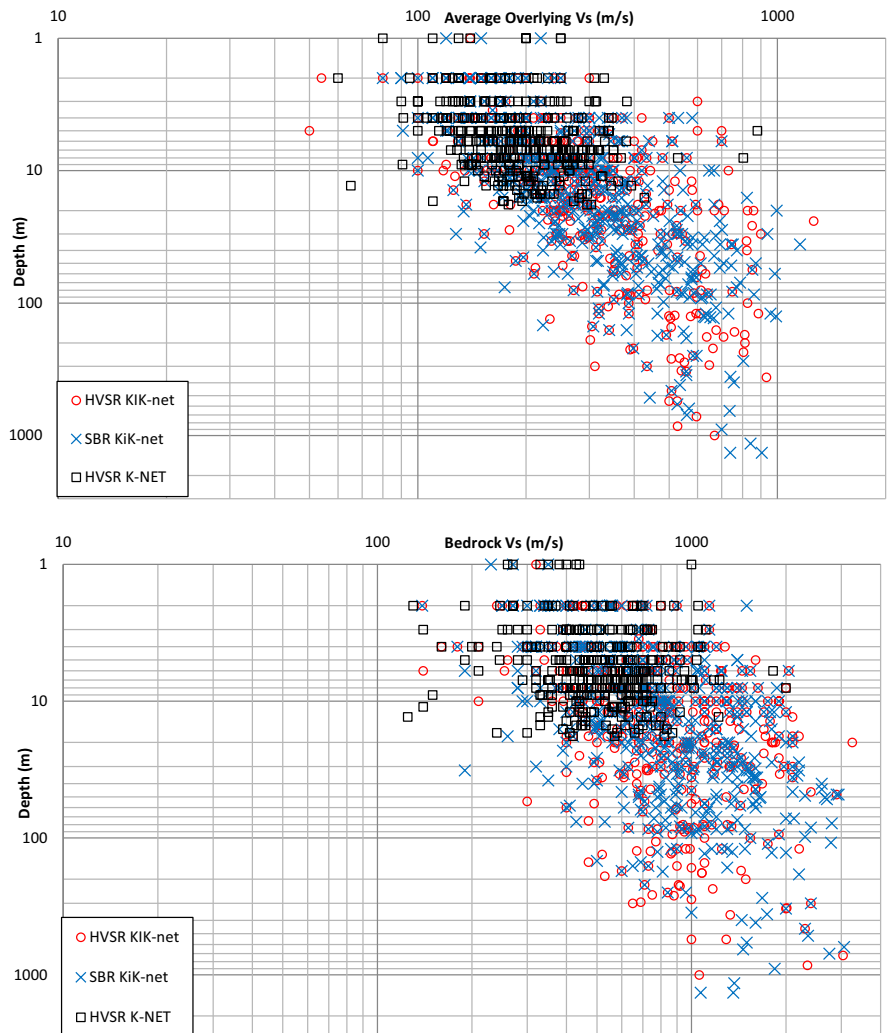
in Eqs. 8 and 9, IC_P and IC_S are the main basics for inferring the reliable bedrock half-space to its corresponding peak frequency.

Generalized nonlinear regression relationships of the f_{HVSR} , estimated using KiK-net sites ($f_{HVSR-KiK}$) and K-NET sites (f_{HVSR-K}), and f_{SBR} versus their corresponding h are superimposed as shown in Fig. 9. Significant scattering in the fundamental resonant frequencies at bedrock depths < 100 m is dominant. These strong deviations of the data points would be analyzed based on seismic site classification and bedrock lithology. Applying the quarter wavelength theory in Fig. 9 will result in identification of shallow and deep sites with average overlying S -wave velocities of 100–200 m/s and 400–800 m/s, respectively. This is a theoretical interpretation of the observed relationships of f versus h , whereas Fig. 10 is showing the

delineated average overlying S -wave velocities obtained from the PS logging seismic velocity structures of KiK-net and K-NET. The most interesting point is that these nonlinear regression relationships of f versus h are strongly corresponding to the average S -wave velocity overlying the bedrock half-space (\bar{V}_S , is illustrated in Eq. 11) versus h (Fig. 10), whereas the bedrock V_S has insignificant relation with their corresponding f versus h (Fig. 10). These results indicate the importance to establish nonlinear regression relationships of f versus h depending on seismic site classification, because there is higher dependency on the \bar{V}_S than the bedrock V_S .

$$\bar{V}_S = h / \sum_{i=1}^n \frac{h_i}{V_{si}} \tag{11}$$

Fig. 10 Average overlying and bedrock (V_S) versus h corresponding to f versus h in Fig. 9



where h is the total thickness of the layers above the bedrock half-space. h_i , V_{si} , and V_{pi} are the thickness, and S -wave velocity, respectively, of each individual layer. n is the number of these layers.

Figure 9 shows the highest scattering in the f versus h at depths < 100 m. Therefore, this generalized f versus h relationship is rebuilt according to different seismic site classifications. Figure 11 shows the f versus h relationships in the main four seismic site class of B, C, D, and E. Reasonable fit could be achieved in the $f_{HVS\text{R}-KiK}$, $f_{HVS\text{R}-K}$, and f_{SBR} versus their corresponding h relationships. Significant differences are present in the f versus h relationships produced from HVS_R and SBR analyses.

Remarkable correlations could be seen in the \bar{V}_S versus h and f relationships as shown in Fig. 11. Poor

fitting could be clearly seen in the bedrock V_S versus h relationships as shown in Fig. 11. This reflects the strong dependency of the resulted $f_{HVS\text{R}-KiK}$, and f_{SBR} on average S -wave velocity structure of the layers over the bedrock half-space. The bedrock V_S has insignificant influence on the resulted fundamental resonant frequency. This interesting point concludes that the presence of the bedrock half-space is determined based on the highest IC_p and IC_s as explained earlier, and not based on the bedrock V_S .

Table 3 summarizes the fitting curve parameters (a and b) with their characterizing maximum \bar{V}_S and the bedrock V_S as depicted from Fig. 11. Among the different lithological groups of different site classes, the high majority of the maximum \bar{V}_S is not exceeding

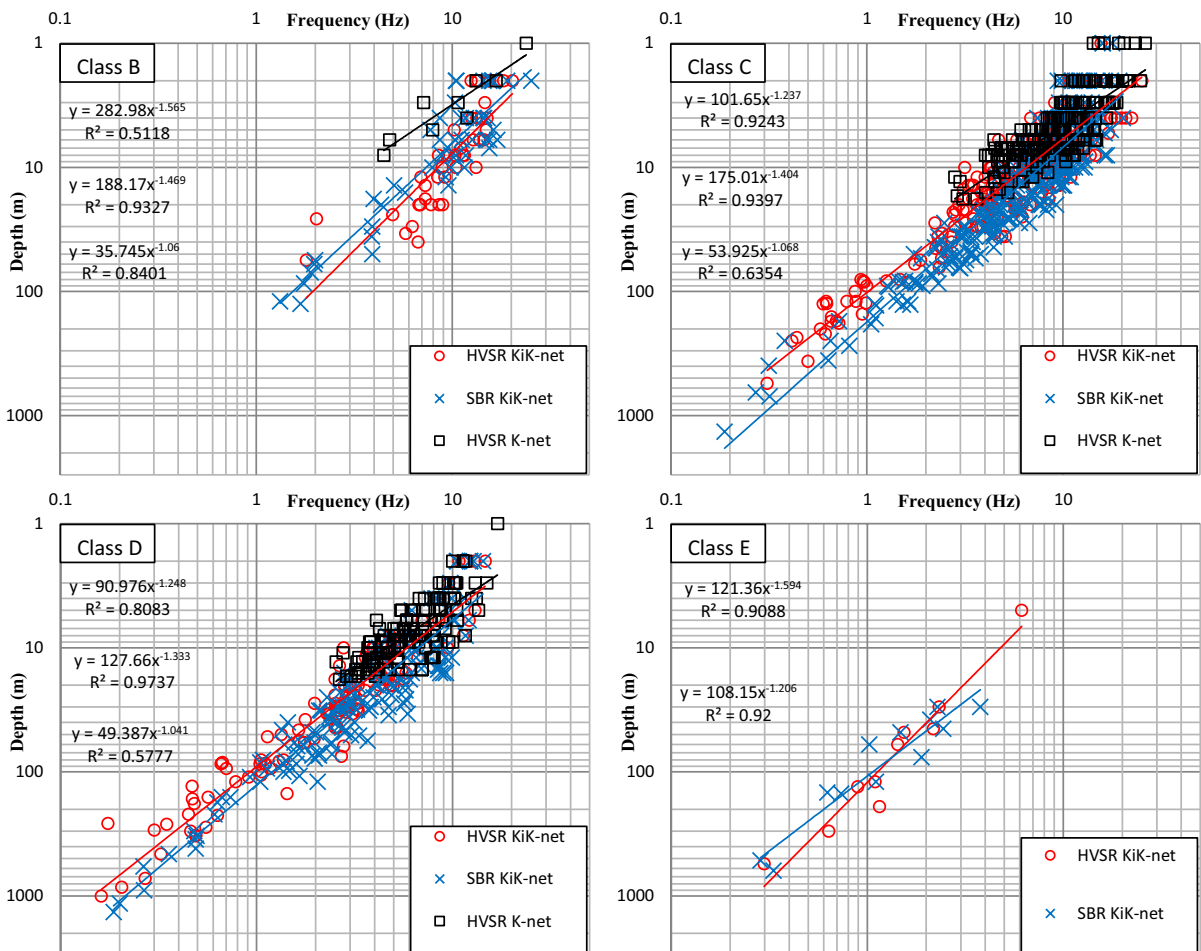


Fig. 11 The f versus h and their corresponding average overlying and bedrock V_S versus h in B, C, D, and E site class

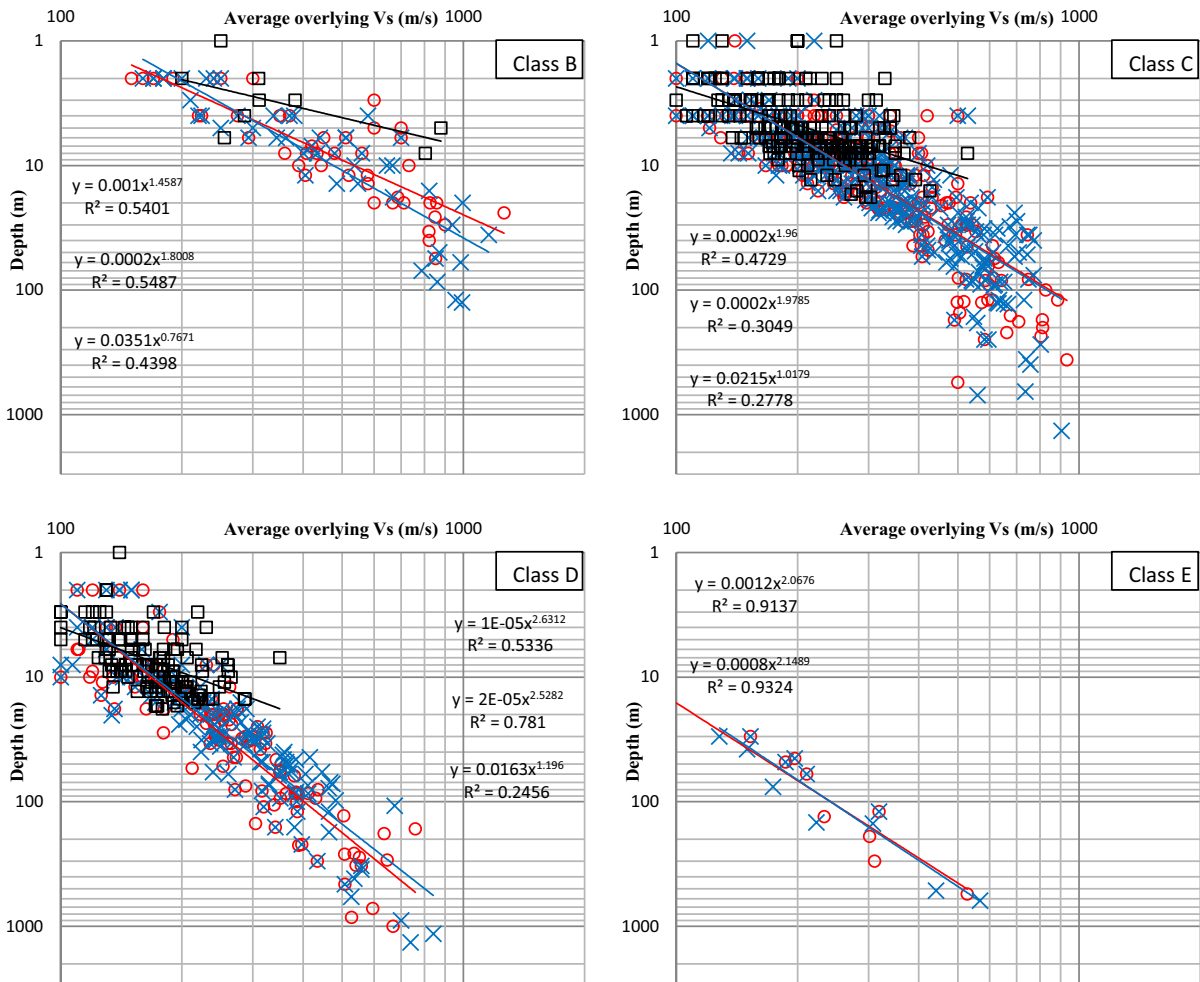


Fig. 11 (continued)

1262 m/s. Moreover, a general gradual decreasing in the maximum \overline{V}_S is observed through site class of B, C, D, and E. Depending on these observations, different gradual ranges for each site class are proposed as shown in Table 4. These gradual ranges and their \pm errors are calculated based on the average values and their standard deviations of the maximum \overline{V}_S in Table 3. Moreover, these gradual ranges of the maximum \overline{V}_S resemble the ranges of V_{s30} in the NEHRP Provision (2000), because the high majority of $f_{HVS\text{R}-KiK}$, $f_{HVS\text{R}-K}$, and f_{SBR} are corresponding to h of ≤ 30 m (refer to Fig. 9). This explains the high importance of studying these nonlinear regression relationships considering the seismic site classification.

It was hoped that the HVSr processing results at K-NET sites would interpret and solve the

strong scattering in the f versus h relationships at h of < 20 m, but it is obvious that $f_{HVS\text{R}-K}$ versus h relationship has strong scattering too (Fig. 9). The resulted parameters of a and b are generally lower than those resulted from the $f_{HVS\text{R}-KiK}$, $f_{HVS\text{R}-K}$, and f_{SBR} versus h relationships (Table 3). This underestimation indicates that the ranges of h and f have strong influence on the resulted a and b coefficients. Also, it is an indication that deep bedrock half-spaces are governing and guiding the overall f versus h relationships.

Ibs-von Seht and Wohlenberg (1999) studied sand formations of class C in western Lower Rhine Embayment, Germany. The ranges of h and f in this previous study were 15–1600 m and 5–0.1 Hz, respectively, and investigated with application of

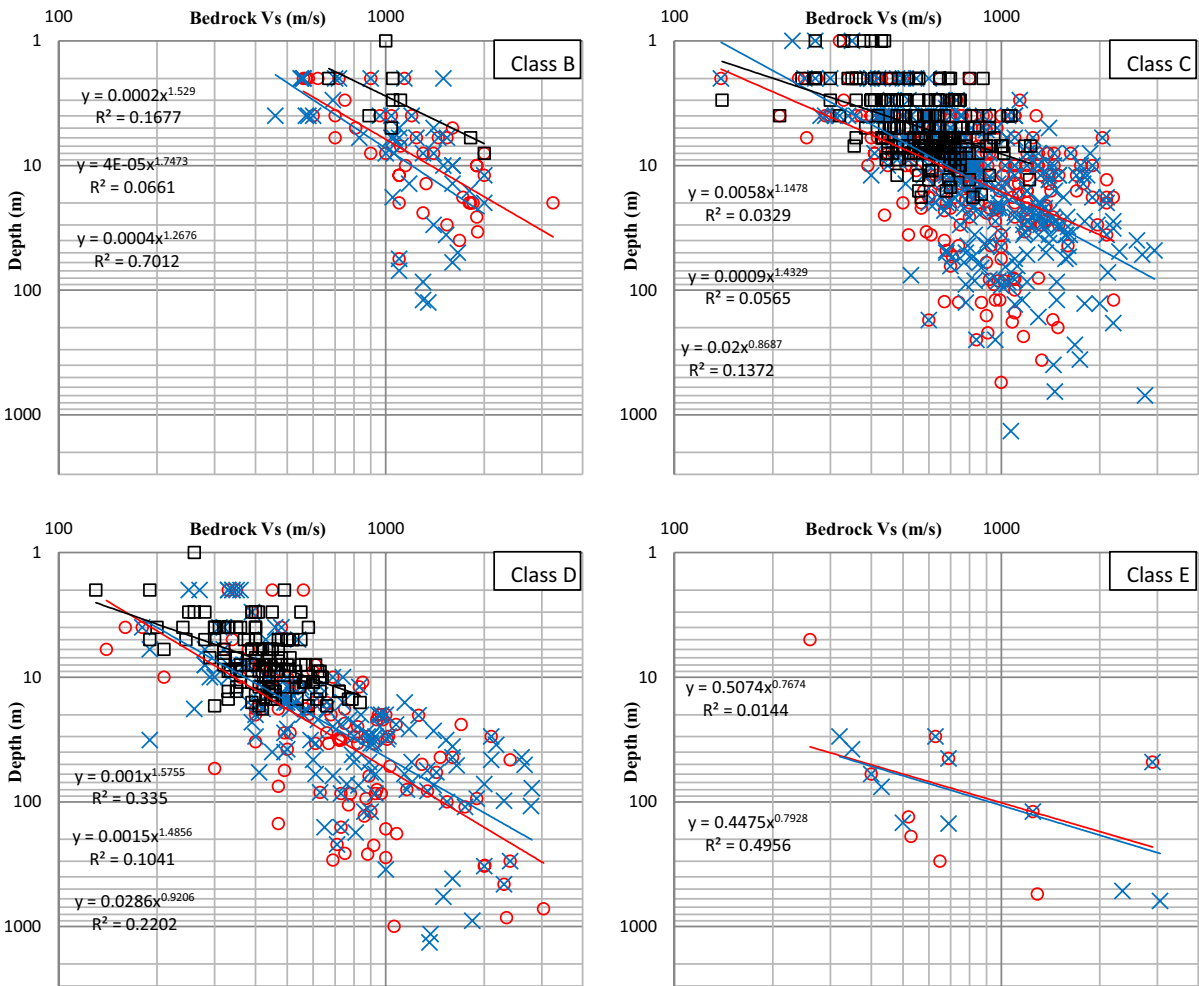


Fig. 11 (continued)

Nakamura’s technique and transfer function technique using microtremor measurements. Scherbaum et al. (2003) presented relationships of \bar{V}_S versus h of sand formations of class C at three arrays near Pulheim, Chorweiler, and Lülldorf in Cologne city area, Germany. Their results consider the uppermost

200–300 m analyzing the fundamental mode Rayleigh wavefield in the frequency range of 0.7–2.2 Hz. Therefore, both studies are used in fair comparison with class C of the present study as shown in Table 5.

D’Amico et al. (2008) mapped the f of the shale sedimentary cover (h) of class C in the city of

Table 3 Summary of correlation coefficients (i.e., a and b) with their characterizing maximum \bar{V}_S and bedrock V_S results through site class of B, C, D, and E

Site class	HVSR-KiK		SBR-KiK		HVSR-K		Max \bar{V}_S	Max. bedrock V_S
	a	b	a	b	a	b		
B	282.98	1.565	188.17	1.469	35.75	1.06	1262	3250
C	101.65	1.237	175.01	1.404	53.93	1.068	933	2940
D	90.976	1.248	127.66	1.333	49.39	1.041	842	3040
E	121.36	1.594	108.15	1.206	—	—	568	3060

Table 4 Proposed ranges of the maximum $\overline{V_S}$ (refer to Table 3) overlying bedrock half-space according to the present study

Site class	Max. $\overline{V_S}$ range
B	$1262 \text{ m/s} \geq \overline{V_S} > 880 \text{ m/s} (\pm 197)$
C	$933 \text{ m/s} \geq \overline{V_S} > 529 \text{ m/s} (\pm 226)$
D	$842 \text{ m/s} \geq \overline{V_S} > 350 \text{ m/s} (\pm 264)$
E	$\overline{V_S} \leq 568 \text{ m/s} (\pm 28)$

Florence, Italy. Their ranges of h and f are $< 5\text{--}153 \text{ m}$ and $0.1\text{--}20 \text{ Hz}$, respectively. The parameters of a and b and their characterizing ranges of $\overline{V_S}$ and bedrock V_S are compared with class C in the present study.

Harutoonian et al. (2013) conducted HVSR micro-tremor measurements in a dynamically compacted gravelly fill area in Western Sydney, Australia. The ranges of h and f are $13.3\text{--}1.2 \text{ m}$ and $4.2\text{--}27 \text{ Hz}$, respectively. Therefore, their parameters of a and b and the characterizing ranges of $\overline{V_S}$ and bedrock V_S are fairly compared with those resulted from HVSR processing of K-NET sites belonging to class D.

Finally, resulted ranges of h and f from Moon et al. (2019) study are $10\text{--}45 \text{ m}$ and $2\text{--}9 \text{ Hz}$, respectively. They studied the bedrock depths of weathered Bukit Timah granite formation in Singapore using microtremor measurements. The sites used in this study belong to site class of D.

Because of similarities in the site information and measurement parameters of these previous

studies and the present study, fair comparison could be achieved considering the site-dependent variability, as shown in Table 5. Interestingly, remarkable similarities could be seen in the parameters of a and b and their characterizing ranges of $\overline{V_S}$ and bedrock V_S . It is important to note that these previous and present relationships are site-specific and highly dependent on each region’s geologic conditions. Therefore, the target of these comparisons is only to introduce the seismic site classification as a crucial controlling factor in establishing the previous and the present nonlinear regression relationships.

5 Conclusions

With the results discussed earlier, it is possible to retrieve the following conclusions. The present study introduces additional improvements to the study conducted by Thabet (2019). These improvements consist of SBR and HVSR processing using database at the 698 KiK-net and the 1045 K-NET sites. The seismic database includes all the available earthquakes with PGAs of $\leq 10 \text{ cm/s}^2$ at each site. Additionally, HVSR and SBR processing using the adopted conjugated records could increase the number of accepted sites due to enhancement in the requirements of SESAME guidelines (Bard and SESAME team 2004). Moreover, the relationships of $\overline{V_S}$ versus h are inversely resembling the relationships of f versus h , whereas the relationships of bedrock V_S versus h

Table 5 Existing correlation coefficients (i.e., a and b) with their characterizing ranges of $\overline{V_S}$ and bedrock V_S results (refer to Table 3)

Lithology/site class	Literature/present study	HVSR–KiK-net		SBR		HVSR–K-NET		$\overline{V_S}$ (m/s)	Bedrock V_S (m/s)
		a	b	a	b	a	b		
C	Ibs-von Seth and Wohlenberg 1999	96 ± 4	1.39 ± 0.03	146 ± 19	1.38 ± 0.21			380–705	2500–3100
	Scherbaum et al. 2003	99	1.31						
		111	1.28						
		102	1.19						
	D’Amico et al. 2008	140	1.17					200–750	> 800
This study	102	1.237	175	1.404	54	1.068	120–813	400–2770	
D	Harutoonian et al. 2013					73	1.17	150–300	> 400
	Moon et al. 2019	92	1.06					200–400	333–584
	This study	91	1.248	128	1.333	49	1.041	60–740	130–2600

have insignificant importance. The shallow and limited ranges of h and f underestimate the parameters of a and b resulted from $f_{HVS\text{R}-K}$ versus h relationship whenever compared with those resulted from the $f_{HVS\text{R}-KiK}$, and f_{SBR} versus h relationships. This indicates that deep bedrock half-spaces are governing and guiding the overall f versus h relationships. Relationships of f_{SBR} versus their corresponding h are strongly resembling relationships of $f_{HVS\text{R}-KiK}$ versus h indicating that SBR analysis is productive and efficient tool to delineate the fundamental resonant frequency. Overall, rebuilding the f_{SBR} and $f_{HVS\text{R}-KiK}$ versus their corresponding h based on site-dependent variability in different lithologies could strongly decrease scattering and deviations of data points. Remarkable correlations could be seen in the $\overline{V_S}$ versus h relationships reflecting the strong dependency of the $f_{HVS\text{R}-KiK}$, $f_{HVS\text{R}-K}$, and f_{SBR} on the $\overline{V_S}$. The high majority of the maximum $\overline{V_S}$ is not exceeding 1262 m/s. The ranges of maximum $\overline{V_S}$ are decreasing gradually through site classes of B, C, D, and E resembling the ranges of the V_{s30} of the seismic site classification according to NEHRP Provision (2000). Therefore, the presence of the bedrock half-space is determined based on the highest IC_p and h without respect to the bedrock $\overline{V_S}$. HVSR inversions based on the diffuse field approach could interpret the presence of the bedrock half-space using the criteria of the highest V_S and h . Interestingly, fair comparisons based on site information and site-dependent variability of different bedrock lithologies between previous relationships of F versus H in the literature and the present study relationships are showing remarkable and reasonable similarities.

It is important to note that these previous and present relationships are site-specific and highly dependent on each region's geologic conditions. The main achievement of the present study is only to introduce the seismic site classification as a crucial controlling factor in establishing the previous and the present nonlinear regression relationships of the depth of high seismic reflection coefficient interface versus the peak resonance frequency and the average overlying S -wave velocity. Practically, inverting the layered S -wave velocity structure is possible using known resonance frequency from HVSR analyses, particularly in regions with deployed strong-motion observation system, and consequently reliable inference of the bedrock depth, average overlying S -wave

velocity, and seismic site classification. As a result, the usefulness of these present nonlinear regression relationships is the possibility to quickly obtain a general idea of the subsurface lithology. Moreover, using these present nonlinear regression relationships based on known subsurface lithology and seismic site classification could be used to provide an initial guess and to constrain ranges of the depths and average overlying S -wave velocity to feed into the HVSR inversion process.

Acknowledgements The author highly appreciated and grateful to the National Research Institute for Earth Science and Disaster prevention (NIED) for making the valuable KiK-net and K-NET data available (<https://doi.org/10.17598/NIED.0004>). The author appreciates and acknowledges the generous, valuable, and constructive comments and suggestions from Prof. Hiroshi Kawase (DPRI, Kyoto University). The author indebted to the Editor-in-Chief, Prof. Mariano Garcia-Fernandez, and the anonymous reviewers for their constructive comments to highly improve the manuscript.

Author contribution The submitting author confirms that he is a single author named in the manuscript, is aware of the submission, and has agreed for the paper to be submitted to the Journal of Seismology. I am acknowledging the consent requirements. I appreciate your careful consideration.

Availability of data and material Any data in this research work would be available upon request immediately.

Code availability Any software application or custom code in this research work would be available upon request immediately.

Declarations

Conflict of interest The author declares no competing interests.

References

- Bard PY, SESAME team (2004) Guidelines for the implementation of the H/V spectral ratio technique on ambient vibrations: measurements, processing and interpretation. SESAME European research project, WP12—Deliverable D23. p 12
- Bindi D, Parolai S, Spallarossa D, Cattaneo M (2000) Site effects by H/V ratio: comparison of two different procedures. *J Earthqu Eng* 4:97–113
- Boore DM (2004) Estimating $V_S(30)$ (or NEHRP site classes) from shallow velocity models (depths < 30 m). *Bull Seismol Soc Am* 94(2):591–597

- Borcherdt RD (1970) Effects of local geology on ground motion near San Francisco Bay. *Bull Seismol Soc Am* 60(1):29–61
- Borcherdt RD (1994) Estimates of site-dependent response spectra for design (methodology and justification). *Earthq Spectra* 10(4):617–653. <https://doi.org/10.1193/1.1585791>
- D'Amico V, Picozzi M, Baliva F, Albarello D (2008) Ambient noise measurements for preliminary site-effects characterization in the urban area of Florence, Italy. *Bull Seismol Soc Am* 98(3):1373–1388. <https://doi.org/10.1785/0120070231>
- Delgado J, Casado CL, Estévez A, Giner J, Cuenca A, Molina S (2000a) Mapping soft soils in the Segura river valley (SE Spain): a case study of microtremors as an exploration tool. *J Appl Geophys* 45:19–32
- Delgado J, Casado CL, Giner J, Estévez A, Cuenca A, Molina S (2000b) Microtremors as a geophysical exploration tool: applications and limitations. *Pure Appl Geophys* 157:1445–1462
- Fäh D, Kind F, Giardini D (2001) A theoretical investigation of average H/V ratios. *Geophys J Int* 145:535–549
- Field EH, Jacob K (1993) The theoretical response of sedimentary layers to ambient seismic noise. *Geophys Res Lett* 20(24):2925–2928
- García-Jerez A, Luzón F, Navarro M, Pérez-Ruiz JA (2006) Characterization of the sedimentary cover of the Zafaraya basin, Southern Spain, by means of ambient noise. *Bull Seismol Soc Am* 96(3):957–967. <https://doi.org/10.1785/0120050061>
- Harutoonian P, Leo CJ, Tokeshi K, Doanh T, Castellaro S, Zou JJ, Liyanapathirana DS, Wong H (2013) Investigation of dynamically compacted ground by HVSR-based approach. *Soil Dyn Earthq Eng* 46:20–29. <https://doi.org/10.1016/j.soildyn.2012.12.004>
- Hinzen KG, Weber B, Scherbaum F (2004) On the resolution of H/V measurements to determine sediment thickness, a case study across a normal fault in the Lower Rhine Embayment, Germany *Journal of Earthquake Engineering* 8(6):909–926. <https://doi.org/10.1080/13632460409350514>
- Horike M, Zhao B, Kawase H (2001) Comparison of site response characteristics inferred from microtremors and earthquake shear waves. *Bull Seismol Soc Am* 91(6):1526–1536. <https://doi.org/10.1785/0120000065>
- Ibs-von Seht M, Wohlenberg J (1999) Microtremors measurements used to map thickness of soft soil sediments. *Bull Seismol Soc Am* 89:250–259
- Kagami H, Duke CM, Liang GC, Ohta Y (1982) Observation of 1- to 5-second microtremors and their application to earthquake engineering. Part II. Evaluation of site effect upon seismic wave amplification due to extremely deep soil deposits. *Bull Seismol Soc Am* 72(3):987–998. <https://doi.org/10.1785/BSSA0720030987>
- Kawase H, Sánchez-Sesma FJ, Matsushima S (2011) The optimal use of horizontal-to-vertical spectral ratios of earthquake motions for velocity inversions based on diffuse field theory for plane waves. *Bull Seismol Soc Am* 101:2001–2004
- Kawase H, Mori Y, Nagashima F (2018) Difference of horizontal to vertical spectral ratios of observed earthquakes and microtremors and its application to S wave velocity inversion based on the diffuse field concept. *Earth, Planets and Space* 70:1. <https://doi.org/10.1186/s40623-017-0766-4>
- Lachet C, Bard PY (1994) Numerical and theoretical investigations on the possibilities and limitations of Nakamura's technique. *J Phys Earth* 42:377–397
- Lermo J, Chavez-Garcia FJ (1993) Site effect evaluation using spectral ratios with only one station. *Bull Seismol Soc Am* 83:1574–1594
- Lermo J, Chavez-Garcia FJ (1994) Are microtremors useful in site response evaluation? *Bull Seismol Soc Am* 84:1350–1364
- Miller RD, Xia J, Park CB, Ivanov J (1999) Multichannel analysis of surface waves to map bedrock. *Lead Edge* 18(12):1392–1396
- Moon S, Subramaniam P, Zhang Y, Vinoth G, Ku T (2019) Bedrock depth evaluation using microtremor measurement: empirical guidelines at weathered granite formation in Singapore. *J Appl Geophys* 171(2019):103866. <https://doi.org/10.1016/j.jappgeo.2019.103866>
- Nagashima F, Matsushima S, Kawase H, Sanchez-Sesma FJ, Hayakawa T, Satoh T (2014) Application of horizontal-to-vertical spectral ratios of earthquake ground motions to identify subsurface structures at and around the K-NET site in Tohoku, Japan. *Bull Seismol Soc Am* 104(5):2288–2302. <https://doi.org/10.1785/0120130219>
- Nakamura Y (1989) A method for dynamic characteristics estimations of subsurface using microtremors on the ground surface. *Q Rep RTRI Jpn* 30:25–33
- Nakamura Y (2000) Clear identification of fundamental idea of Nakamura's technique and its application. *Proceedings of the XII World Conf. Earthq. Engrg.* Auckland, p 8
- NEHRP (2000) Recommended provisions for seismic regulations for new buildings and other structures, part 1: provisions, prepared by the Building Seismic Safety Council (BSSC) for the federal emergency management agency. Report FEMA 368. NEHRP, Washington, p 2001
- Nath SK (2007) Seismic microzonation framework—principles and applications. *Proc. Workshop on Microzonation*, Indian Institute of Science, Bangalore, 26 – 27 June 2007, India. pp 9–35
- Nogoshi M, Igarashi T (1970) On the propagation characteristics estimations of subsurface using microtremors on the ground surface. *J Seismol Soc Jpn* 23:264–280
- Nogoshi M, Igarashi T (1971) On the amplitude characteristics of microtremor (part 2). *J Seismol Soc Jpn* 24:26–40
- Özalaybey S, Zor E, Ergintav S, Tapırdamaz MC (2011) Investigation of 3-D basin structures in the İzmit Bay area (Turkey) by single-station microtremor and gravimetric methods. *Geophys J Int* 186:883–894. <https://doi.org/10.1111/j.1365-246X.2011.05085.x>
- Parolai S, Bormann P, Milkert C (2002) New relationships between V_s , thickness of sediments, and resonance frequency calculated by the H/V ratio of seismic noise for Cologne Area (Germany). *Bull Seismol Soc Am* 92:2521–2527
- Régnier J, Cadet H, Bonilla L, Bertrand E, Semblat J (2013) Assessing nonlinear behavior of soils in seismic site response: statistical analysis on KiK-net strong-motion data. *Bull Seismol Soc Am* 103(3):1750–1770. <https://doi.org/10.1785/0120120240>

- Rong MS, Wang ZM, Woolery EW, Lyu YJ, Li XJ, Li SY (2016) Nonlinear site response from the strong ground-motion recordings in western China. *Soil Dyn Earthq Eng* 82:99–110
- Sánchez-Sesma FJ, Rodríguez M, Iturrarán-Viveros U, Luzón F, Campillo M, Margerin L, García-Jerez A, Suarez M, Santoyo MA, Rodríguez-Castellanos A (2011) A theory for microtremor H/V spectral ratio: application for a layered medium. *Geophys J Int* 186:221–225
- Satoh T, Kawase H, Sato T (1995) Evaluation of local site effects and their removal from borehole records observed in the Sendai Region, Japan. *Bull Seismol Soc Am* 85(6):1770–1789
- Satoh T, Kawase H, Iwata T, Higashi S, Sato T, Irikura K, Huang HC (2001a) S-wave velocity structure of the Taichung Basin, Taiwan, estimated from array and single-station records of microtremors. *Bull Seismol Soc Am* 91(5):1267–1282. <https://doi.org/10.1785/0120000706>
- Satoh T, Kawase H, Matsushima S (2001b) Differences between site characteristics obtained from microtremors, S-waves, P-waves and codas. *Bull Seismol Soc Am* 91:313–334
- Scherbaum F, Hinzen KG, Ohrnberger M (2003) Determination of shallow shear wave velocity profiles in the Cologne, Germany area using ambient vibrations. *Geophys J Int* 152(3):597–612
- Thabet M, Nemoto H, Nakagawa K (2008) Variation process in stiffness inferred by nonlinear inversion during mainshocks at Kushiro Port vertical array site. *Earth Planet Sp* 60:581–589. <https://doi.org/10.1186/BF03353121>
- Thabet M (2019) Site-specific relationships between bedrock depth and HVSR fundamental resonance frequency using KiK-net data from Japan. *Pure Appl Geophys* 176(11):4809–4831. <https://doi.org/10.1007/s00024-019-02256-7> (2019 Springer Nature Switzerland AG)
- Thabet M (2021) Nonlinearity evaluation considering the uncertainty of S-wave velocity based on total stress analyses and diffuse field assumption: the Mw 9.1 great Tohoku Taiheiyō-Oki earthquake at 05:46 UTC on 11 March 2011. *Journal of Seismology* 25(2):535–574. <https://doi.org/10.1007/s10950-020-09974-9>
- Tao Y, Rathje E (2020) The importance of distinguishing pseudo-resonances and outcrop resonances in downhole array data. *Bull Seismol Soc Am* 110(1):288–294. <https://doi.org/10.1785/0120190097>
- Tün M, Pekkan E, Özel O, Guney Y (2016) An investigation into the bedrock depth in the Eskisehir Quaternary Basin (Turkey) using the microtremor method. *Geophys J Int* 207(1):589–607. <https://doi.org/10.1093/gji/ggw294>
- Wen KL, Chang TM, Lin CM (2006) Identification of nonlinear site response using the HVSR method. *Terr Atmos Ocean Sci* 17(3):533–546
- Yamanaka H, Takemura M, Ishida H, Niwa M (1994) Characteristics of long-period microtremors and their applicability in exploration of deep sedimentary layers. *Bull Seism Soc Am* 84:1831–1841
- Zhu C, Pilz M, Cotton F (2020) Evaluation of a novel application of earthquake HVSR in site-specific amplification estimation. *Soil Dyn Earthq Eng* 139:106301. <https://doi.org/10.1016/j.soildyn.2020.106301>

Publisher's note Springer Nature remains neutral with regard to jurisdictional claims in published maps and institutional affiliations.